On the use of acoustic methods for the detection of electrostatic capture of diaphragm in capacitive MEMS microphones

This article has been accepted for publication in a future issue of this journal, but has not been fully edited. Content may change prior to final publication. Citation information: DOI 10.1109/TCPMT.2021.3107225, IEEE Transactions on Components, Packaging and Manufacturing Technology

On the use of acoustic methods for the detection of electrostatic capture of diaphragm in capacitive MEMS microphones

Gergely Hantos, *Student Member, IEEE*, Gergely Simon, *Student Member, IEEE,* and Marc P.Y. Desmulliez, *Senior Member, IEEE*

***Abstract*— Most mobile phones today have capacitive micro-electromechanical systems (MEMS) microphones that use either single or dual diaphragm. Methods to detect failures easily and non-invasively have become of critical importance for microphones mobile phone manufacturers as a basis for built-in self-test (BIST) and self-repair (BISR) strategies. In that regard, a four-layer framework is presented that includes lumped element modelling (LEM), failure mode simulation, failure mode discrimination and recovery. The frequency response of the microphone is taken as the main output to analyse. To experimentally validate this framework, this article provides a failure mode induction method based on bias voltage sweeping and four new techniques, based solely on acoustic measurements to discriminate the states of electrostatic capture for single diaphragm capacitive MEMS microphones. These include a) analysis of an acoustic signature that is unique to electrostatic capture based on cosine similarity analysis, b) -3 dB point measurement, C) +3 dB point measurement, and d) cluster analysis. Measurement of pull-in voltage and snapback voltage ranges is further demonstrated based on sensitivity measurements in laboratory conditions and response magnitude and noise power measurements in non-laboratory conditions. Up to 100% success rate in detecting electrostatic capture of diaphragm is reported for this type of device.**

***Index Terms*— Acoustic MEMS, microphone, failure induction, built-in self-test, BIST, built-in self-repair, BISR, capacitive microphone.**

I. Introduction

THE detection, characterization and understanding of the time behaviour of system failures is critical for the diagnosis and prognosis of health of assets in all industrial sectors. Obtaining empirical data can be however challenging if there are insufficient faulty devices at hand as is the case for returns from some customer products. A typical remedial approach to acquire data is to artificially induce the faults. In the case of micro-electro-mechanical systems (MEMS), this procedure is documented in various JEDEC standards such as JESD94 [1] and JEP148A [2]. These standards allow for various measurements such as lifetime tests to be undertaken, whereby a device is declared unsuitable once a threshold value regarding one of its parameters has been reached. Little guidance is however provided as to how the device behaviour changes during the onset of failures. This article aims to provide, in the specific case of capacitive MEMS microphones, a set of methods that allow to model and study real-time deviations of output device responses from normal operating behaviour.

There are various types of causes of failures affecting MEMS microphones with some inducing catastrophic phone failures, others changing the response of the device in a way that allows the determination of the failure involved [3]. A common issue for capacitive MEMS microphones is electrostatically induced stiction, also referred to as electrostatic capture, which is the snapping, beyond a threshold voltage value, of the diaphragm and the backplate forming the plates of a microphone capacitor as shown in Fig. 1[4].

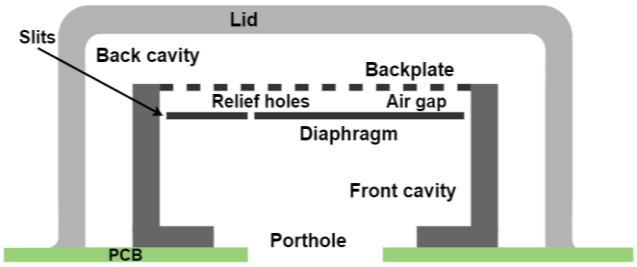

Fig. 1. Simplified schematic of a single diaphragm MEMS microphone.

Assuming that voltage values can be varied, two voltage thresholds can be established: the pull-in voltage, V_{pi}, which refers to the voltage for which the plates snap together, and the snapback voltage, V_{sb}, that describes the voltage for which the plates are released from the captured state. The physics related to this phenomenon has been intensively studied and results obtained have been used to avoid membrane collapse for

Manuscript received XX XX, 2021; accepted XX XX, 2021. Date of publication XX XX, 2021; date of current version XX XX, 2021. Recommended for publication by XXXXX XXXXX upon evaluation of reviewers' comments.

This work was funded in part by the Engineering and Physical Sciences Research Council (EPSRC) under Grant #1799140 – Centre for Doctoral Training in Embedded Intelligence (CDT-EI).

G. Hantos, M. Desmulliez and G. Simon are with the School of Engineering & Physical Sciences, Institute of Sensors, Signals & Systems, Heriot-Watt University, Edinburgh Campus, Edinburgh, Scotland, EH14 4AS (e-mails: gbh1@hw.ac.uk, m.desmulliez@hw.ac.uk, gsimon89@gmail.com).

This article has been accepted for publication in a future issue of this journal, but has not been fully edited. Content may change prior to final publication. Citation information: DOI 10.1109/TCPMT.2021.3107225, IEEE Transactions on Components, Packaging and Manufacturing Technology

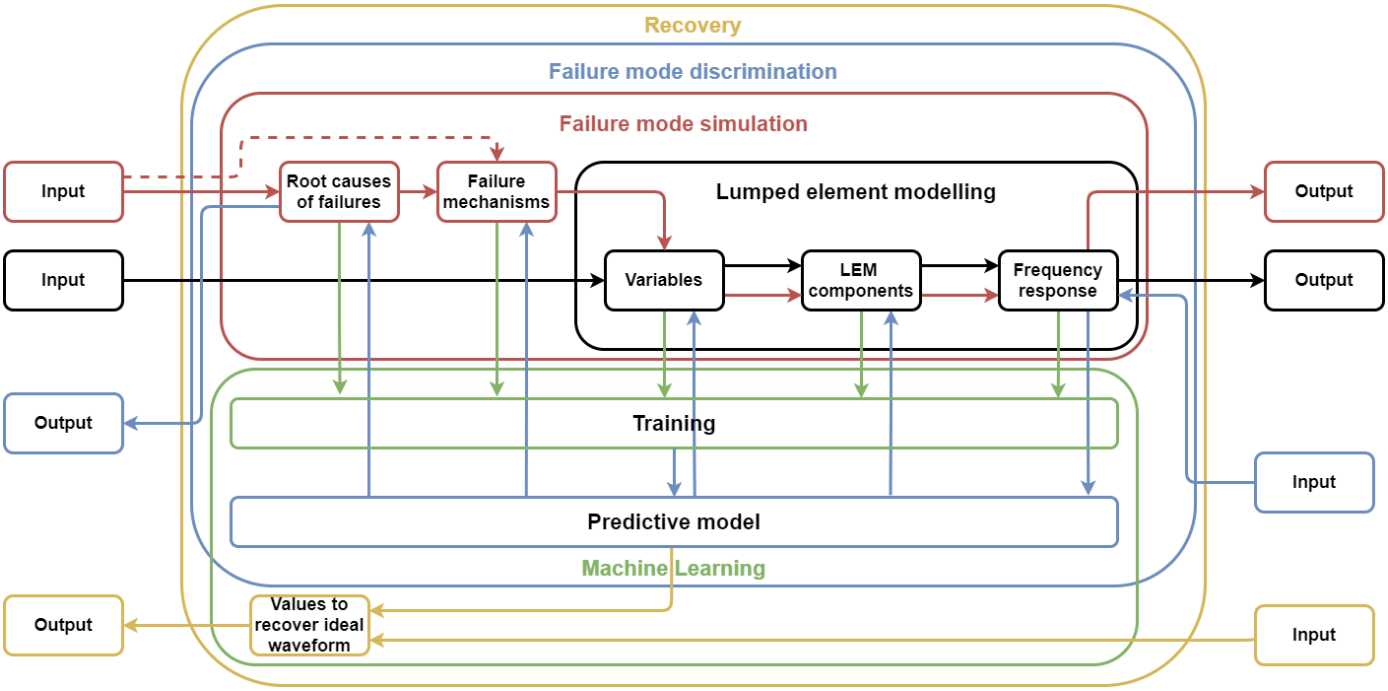

Fig. 2. Illustration of the four-layer framework

reliable operation of electrostatic driven capacitive MEMS [5]. Taking into account changes in environmental operating conditions and size-dependent material properties at the microscale, it is possible to define boundary conditions within which safe operation of the microphone is guaranteed. However, due to material degradation, sudden accidental damage or unexpected environmental effects, voltage thresholds may change along with the magnitude response of the Device Under Test (DUT). Reliability issues occurring under such conditions and during device operation require therefore fault detection, fault discrimination and correction techniques that can be deployed in real-time. As a basis to answer these requirements for BIST and BISR solutions that can be executed at assembly stage and/or in field, a four-layer framework shown in Fig. 2 was developed, with each layer building on the previous one and includes: Lumped element modelling (Black layer), Failure mode simulation (Red layer), Failure mode discrimination (Blue layer) and Recovery (Yellow layer). The feasibility of the framework is supported by experimental data acquired through failure mode induction as presented in ESTC2020 [6]. The failure mode recognition involves four discrimination methods that allow the precise characterization of failure behavior and the detection of electrostatic capture without additional circuitry. The discrimination methods are based on acoustic fingerprint as detailed later, -3 dB point, +3 dB point measurements and a data clustering algorithm. While one of the methods is based on the same principle presented in the sensitivity work of Walser *et al.* [7], which was conducted in laboratory settings, this technique is developed further with demonstration within an in-field setup. Our methods are suitable for deployment both in laboratory conditions during the manufacturing or product return stages, or during device operation, making them ideal candidates as BIST methods. While other BIST solutions, that rely on the electrostatic actuation of the sensing element [8], are mainly transducer specific, our methods allow also backwards compatibility as they are software based with the only information required being the acoustic data coming from the MEMS microphone itself. The lumped element model is introduced in section II along with a detailed explanation of the failure mode simulation. The capture discrimination techniques are explained in section III along with their efficiencies. Discussion of the obtained results is presented in Section IV followed by conclusions in Section V.

II. Microphone Model and Failure Mode Simulation

A. Lumped element model

The core (black) layer of the four-layer framework builds on the lumped element modelling (LEM) of the microphone [9], as shown in Fig. 3. Each of the components include geometrical and material properties that characterise each element of the microphone.

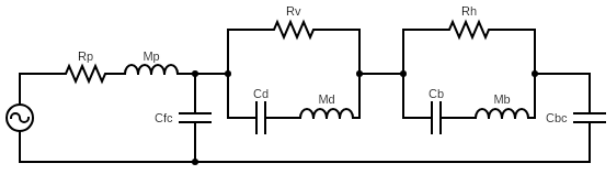

Fig. 3. Lumped parameter model of a MEMS microphone [9]. R_p and M_p are the porthole resistance and mass; R_v is the combined relief hole and vent resistance; C_d and M_d are the compliance and mass of the diaphragm; R_h is the backplate hole resistance; C_b and M_b are the compliance and mass of the backplate; C_{fc} and C_{bc} are the front cavity and back cavity compliances, respectively.

The model shown in Fig. 3 represents an analog bottom port capacitive MEMS microphone with a single backplate and

single diaphragm having the same transducer structure as illustrated in Fig. 1. The experimental work presented in this paper was carried out on such identical devices.

B. *Failure mode simulation*

The red layer of the four-layer framework simulates failure modes by altering the numerical values of the LEM components used in the black layer. To quantify the differences between the frequency responses of a pristine and faulty microphone, the following key response parameters of the frequency response are considered: sensitivity, defined as the electrical response of the device to a given sound pressure level normally measured at 1 kHz at 94 decibels (dB) sound pressure level (SPL) [10], [11], the frequencies at which responses of the microphone are at -3 dB point, also called roll-off frequency, and +3 dB point with respect to the value of the sensitivity.

Effect of failures on the components of the LEM of the microphone and the device frequency response can be illustrated in the case of electrostatic stiction, for example. Assuming an infinitely stiff backplate, the only altered parameter is the acoustic compliance of the diaphragm, which is calculated as [12] [13]:

$$C_d = \frac{32 \cdot {A_{dia}}^2}{\pi^6 \cdot \sigma_d \cdot h_d} \quad (1)$$

where σ_d is the built-in stress of the diaphragm, h_d is the thickness of the diaphragm and A_{dia} is the total diaphragm area. As a result of elevated V_{bias}, the increased electrostatic forces impose additional stress on the membrane which leads to the modification of the diaphragm compliance. This has an impact not only on the output response magnitude, but also on the sensitivity [14], the ±3 dB points, the resonance frequency, F_{res}, of the microphone and its quality factor Q [6], as

$$F_{res} = \frac{1}{2\pi\sqrt{LC}} \quad (2)$$

$$Q = \frac{1}{2\pi RC} \quad (3)$$

where C is the total acoustic compliance of the front cavity, back cavity and diaphragm; L is the total acoustic mass of the porthole and diaphragm, and R is the total acoustic resistance of the porthole, thin air film in the airgap and backplate holes. The roll-off frequency:

$$F_{roll-off} = \frac{1}{2\pi R_v C_{all}} \quad (4)$$

where R_v is the combined acoustic resistance of the relief holes and every single other slit and cavity that create a path of air that bypasses the diaphragm, is also a function of the properties of the diaphragm through C_{all} which is the total acoustic compliance of the diaphragm and back cavity. As (4) is dominated by the back-cavity compliance, only a minimal change would be expected in the low frequency roll-off as the stress of the diaphragm is modified. As the diaphragm is deflected, the slits grow in surface area, leading to an increased volume of air in the cavities bypassing the diaphragm causing the combined acoustic resistance, R_v, to decrease in magnitude. In this work, a ten-fold increase in diaphragm stress is estimated to cause 10% increase in slit dimensions. The effects of increased diaphragm stress on the normalized frequency response of the microphone with slit expansion are shown in Fig. 4.

The normalized frequency response at 1 kHz with respect to that of a pristine microphone allows the observation of the change in the other key response parameters of the frequency response in the low and high frequency regions. The increased stress of the diaphragm results in a slight increase in the ±3dB points. The shift in the -3dB point is not significant enough to affect the sensitivity of the mobile phone.

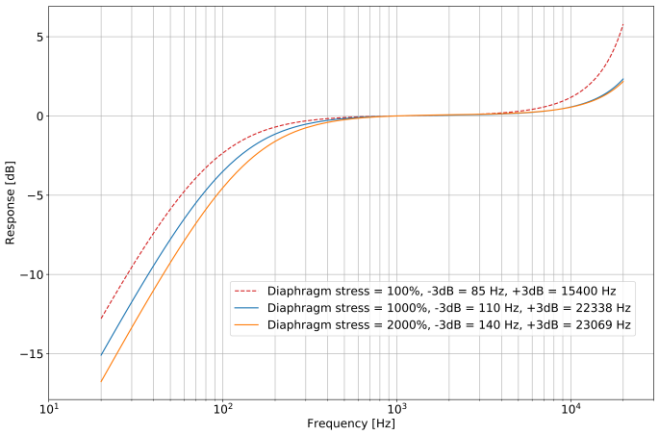

Fig. 4. Simulation of three frequency responses with increasing diaphragm stresses, normalised at 1 kHz with diaphragm stresses and ±3 dB points indicated. The red dotted line shows simulation of the frequency response of a pristine microphone with the nominal stress value used for the simulation.

Electrostatic stiction can be simulated by changing the bias voltage, V_{bias}, as described in [6], and by recording the frequency response of the microphone at each change of the bias voltage. Stiction occurs when V_{bias} reaches V_{pi}, which depends on the transducer geometry and its physical properties [5]. As stiction results in noticeable increase of membrane deflection, simulations can be carried out to capture the trends of the expected outcome. A simulation of a bias voltage sweep for given capture and snapback ranges is shown in Fig. 5. The numbers indicate the order where the simulations were carried out. The blue dots in the simulation indicate an increase in response magnitude with increased bias voltage. The orange crosses show that, once stiction happened, increasing the bias voltage would only further stiffen up the membrane thus reducing compliance and response magnitude. Snap back is seen to occur between measurements 10 and 11.

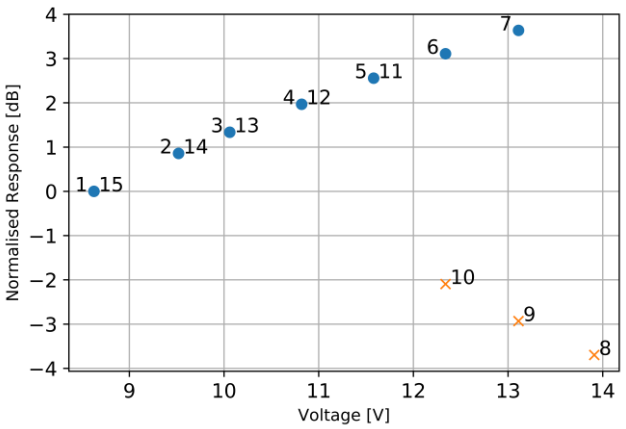

Fig. 5. Simulated normalised frequency response as a function of V_{bias} for a given V_{pi} of 13.11V and V_{sb} of 11.58V. The magnitudes of the response are captured at 1 kHz and are normalised to the response at the beginning of the sweep, marked with 1. Labelled numbers indicate the result of the response for each increment of the bias voltage during its increase and then decrease. Blue dots indicate the instances without and orange crosses indicate the instances with stiction

C. *Failure mode induction and measurement*

The induction of stiction in our experiments followed closely the simulation of such a failure mode as described previously. As the bias voltage of the microphone can be controlled externally, the method did not require any modification of the package or the transducer. The steps of the measurement procedure are shown in Fig. 3 in [6]. The measurements were recorded on two different experimental setups. Experimental setup 1 used a standard acoustic measurement laboratory setup to measure the frequency response and to provide sensitivity related data. Experimental setup 2 was designed to extract the device response and background noise in a real-life environment. Detailed descriptions of the two setups are given in [6].

III. Experimental Validation and Failure Mode Discrimination

This section focuses on the recognition or discrimination of the measured frequency responses related to electrostatic stiction. The simulation data acquired using the red layer of the four-layer framework laid the foundations for the expected deviations in the frequency response resulting from this failure mode. This section introduces four different methods used to analyse the experimental data and discriminate various failure modes from electrostatically induced stiction.

A. *Dataset related to experimental setup 1*

The sensitivity and ±3 dB points of the microphones were measured in this experimental setup. These parameters can be found in specifications sheets of most microphone manufacturers and are excellent indicators of certain issues described further in this article.

1) *Impact on key response parameters:*

Sensitivity deviationin the absence of stiction, it is well known that the sensitivity is a linear function of the bias voltage [12], [15], [16]. An example is provided in Fig. 6 where the number next to the markers (dots or crosses) indicates the order where the measurement was executed. One number only is indicated as most of the markers belonging to the same measurement overlap. Measurements 9, 10, 11 have multiple markers since, during the same measurement sequence, different measurement values of the sensitivity were recorded. Unlike non-electrostatically induced stiction, electrostatic capture is a dynamic effect, and it is challenging to identify how much of the membrane is in contact with the dimples of the backplate. As the electrostatic force increases with voltage between the plates, it is suspected that a larger part of the membrane surface is in contact with the backplate dimples. It is not guaranteed however that the exact same behaviour occurs for the same value of the bias voltage. Like the simulated data, the recorded data exhibit typical hysteretic behaviour [17]. In this figure, minimum and maximum voltage ranges for capture are clearly distinguishable. Fig. 6 shows a traditional hysteresis curve as the order of events is clear: the capture event happens between measurement 8 and 9 and the snapback event happens at measurement 12.

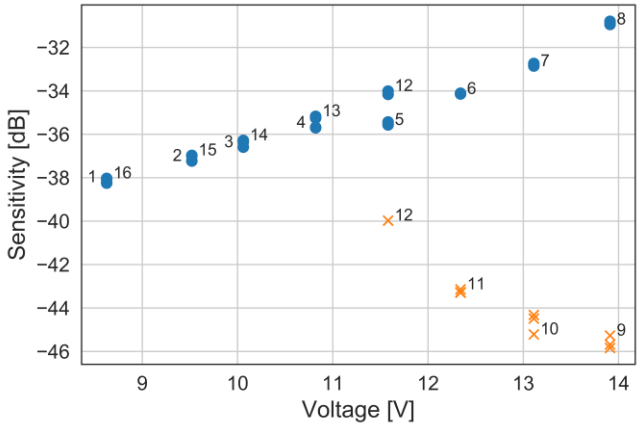

Fig. 6. Sensitivity as a function of voltage for microphone number 80 with the order of experiments indicated. Orange crosses show records with electrostatic capture of the diaphragm (stiction) while blue dots show instances without capture.

2) *Impact on ±3 dB points*

In the state of capture, the diaphragm is forced into a prolonged deflection. The value of the diaphragm compliance is therefore expected to change. This change is observable in both low and high frequency ranges as the -3 dB and the +3 dB points are both influenced by the diaphragm compliance. From (4) it is clear that a lower diaphragm compliance value results in a higher low frequency roll-off. The +3 dB point is affected by (2) and (3). Considering that every other parameter except the diaphragm compliance is constant, a lower diaphragm compliance increases the resonance frequency and quality factor resulting in a narrower resonance peak and increase of the +3 dB point.

Fig. 7 shows the measurements of the normalised frequency response of the same microphone under two different bias voltages.

This article has been accepted for publication in a future issue of this journal, but has not been fully edited. Content may change prior to final publication. Citation information: DOI 10.1109/TCPMT.2021.3107225, IEEE Transactions on Components, Packaging and Manufacturing Technology

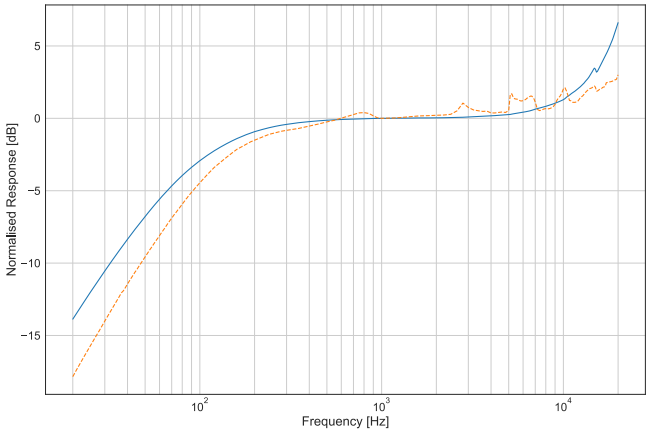

Fig. 7. Measurements of the frequency response on the same microphone with different bias voltages. The blue curve (solid line) shows a measurement in a state of non-capture while the orange curve (dotted line) shows a measurement in the state of capture. The two graphs are normalised at 1 kHz to allow comparison of the waveforms.

The blue (solid line) waveform shows a normal response without capture; the orange (dotted line) curve is a waveform where the V_{pi} threshold is exceeded. The graph in the state of capture has 3 indicators that are of interest for this work:

- The low frequency response is damped
- The high frequency response is damped
- The curve shows fluctuations above 1 kHz

Observations regarding the high and low frequency responses correspond to measurements obtained in Fig. 8 and Fig. 9, respectively The roughness above 1 kHz is explained in detail in section III.A.3).

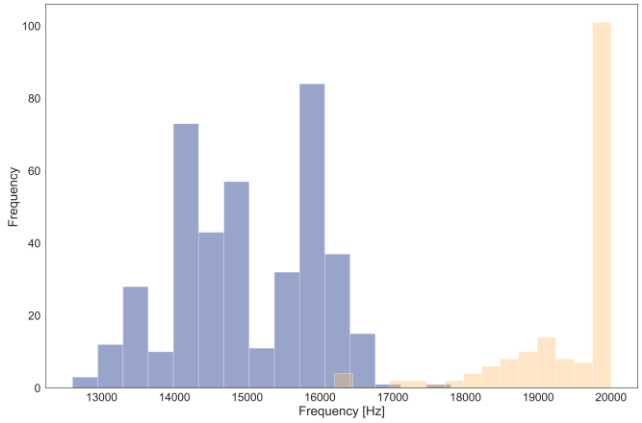

Fig. 8. Distribution of +3 dB point in no-capture state (blue, left) and in capture state (orange, right). Frequency in the vertical axis indicates the number of occurences at the frequency stated on the horizontal axis.

As shown in Fig. 8, the +3 dB points lie between 12,600 Hz and 16,800 Hz. When forced into a state of capture this range shifts to 15,800 Hz to 20,000 Hz, which is the upper limit of the observation enabled by the experimental setup. It is probable that some +3 dB points lie above this limit. This clear shift in frequency combined with a negligible overlap between the two ranges indicate a significant influence of the diaphragm compliance on the +3 dB point.

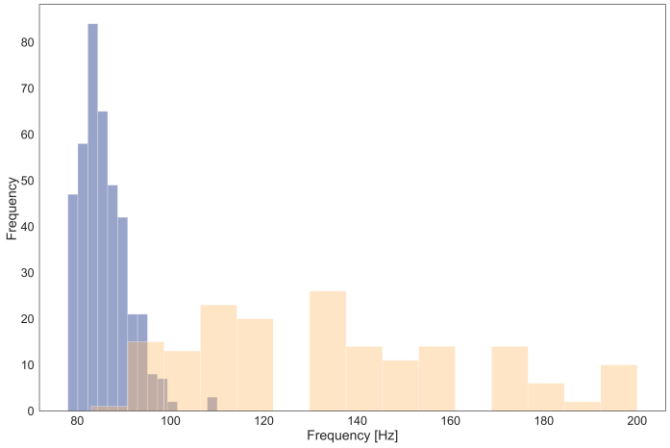

Fig. 9. Distribution of -3 dB point in no-capture state (blue, left) and in capture state (orange, right). Frequency in the vertical axis indicates the number of occurences at the frequency stated on the horizontal axis.

Similar results occur regarding the -3 dB point as shown in Fig. 9. The devices not in a state of capture have a low frequency roll-off between 78 Hz and 110 Hz. In a state of capture this range increases to 83 Hz to 200 Hz. The impact on the low frequency roll-off is clear, however an overlap is present between the two ranges. This is presumably because the magnitude of shift in the key response parameter is not large enough to compensate for the width of the distribution.

3) Roughness above 1 kHz

The recorded frequency responses contain a unique identifier in the high frequency region and which only appears when the device is in a state of capture as shown in Fig. 7. The roughness of the curve above 1 kHz appears on every device in the state of capture.

Cosine similarity algorithm was utilized as a metric of similarity between the two sets of curves [18]. The process of capture identification based on roughness-based similarity measurement is as follows. A sample data row is selected from the capture data records, then cosine similarity is measured for the whole dataset using the selected record taken as a reference. Fig. 10 shows the results of cosine similarity-based capture state recognition. Data drawn in orange (left) show the capture data, blue data (right) are the non-capture data. The two distributions are clearly distinguishable. The required numerical precision is set by the number of datapoints in the vectors used for cosine similarity analysis, thus ultimately the dimensionality of the vectors. We found that for our application a four decimal precision was sufficient.

This article has been accepted for publication in a future issue of this journal, but has not been fully edited. Content may change prior to final publication. Citation information: DOI 10.1109/TCPMT.2021.3107225, IEEE Transactions on Components, Packaging and Manufacturing Technology

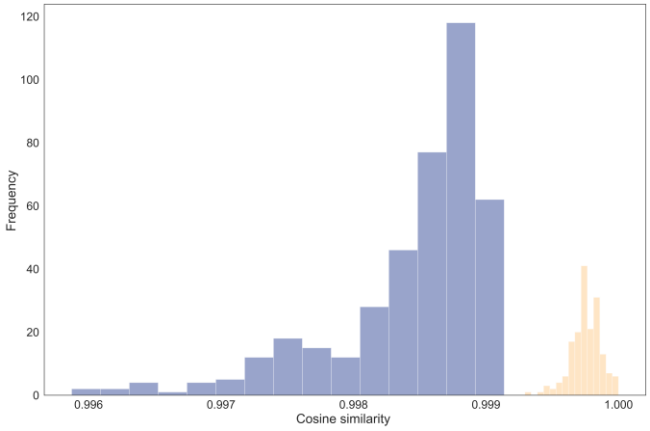

Fig. 10. Cosine similarity distribution of data rows using a capture row as a reference. Blue data shows similarity to data without capture, orange data shows similarity to data with capture.

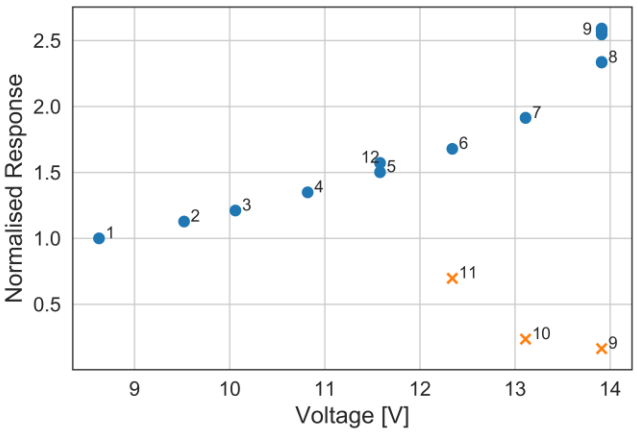

Fig. 11. Voltage - response graph for a single microphone with the order of experiments indicated. Orange crosses show captured instances while blue dots show instances without capture

B. *Dataset related to experiment 2*

Setup 2 is evaluated using different metrics. The main issues with the setup include the difficulty to calculate the exact sensitivity without a reference microphone, and the changing position of the microphones with respect to the main speaker located above the microphones.

Because of the lack of a reference microphone, the output of the measurements using the headphone speaker is better defined as a device response at 1 kHz (from now on referred to as response). The next issue comes from the construction of most headphones which are not designed to stay in place with extreme accuracy while being in a folded state. The flexibility of the structure causes differences in the relative position of the microphone with respect to the speaker when the setup is moved. A similar cosine similarity analysis of the recorded responses confirms however that the change in relative position is negligibly small if the setup is left undisturbed.

As the setup is moved between sets of measurements, different measurements sets cannot be compared with each other; only data from the same experiment can be used for relative measurements.

1) *Impact on the response level*

Similarly to the experimental setup 1, the response of the device is expected to change with shift in bias voltage as shown in Fig. 11. Each dot shows a single point of measurement for the normalised device response measured at 1 kHz.

The recorded data exhibits hysteretic behaviour and the minimum and maximum voltage ranges for capture are clearly distinguishable. Electrostatic capture happens during the recordings of measurement 9 as there are measurement instances in both capture and no-capture states while the snapback happens between measurements 11 and 12. The graphs in Fig. 6 and c are very similar. The measurements were carried out using the same microphone. The only difference between the hysteretic behaviour of the two figures is the snapback range that is probably caused by the different measurement conditions.

2) *Impact on noise power*

There are various noise sources present in a MEMS microphone [19]. While a higher bias voltage is usually utilized to increase the Signal to Noise Ratio (SNR) [20], an acoustic noise source located close to a microphone will be picked up as a signal. If we assume an acoustic background noise with constant power, this “signal” can be used to track the state of capture even without using an input signal noticeable by humans. Noise power measurements were executed in a manner similar to signal response measurements without any dedicated input signal to the speaker. With the speaker being silent it was assessed whether the noise level would change with a changing bias voltage. Average noise power was calculated from the FFT spectrum of the recordings. Fig. 12 shows the results of the noise power measurement for a single microphone. The results are very similar to those in Fig. 11 and the captured instances are just as easy to distinguish.

This article has been accepted for publication in a future issue of this journal, but has not been fully edited. Content may change prior to final publication. Citation information: DOI 10.1109/TCPMT.2021.3107225, IEEE Transactions on Components, Packaging and Manufacturing Technology

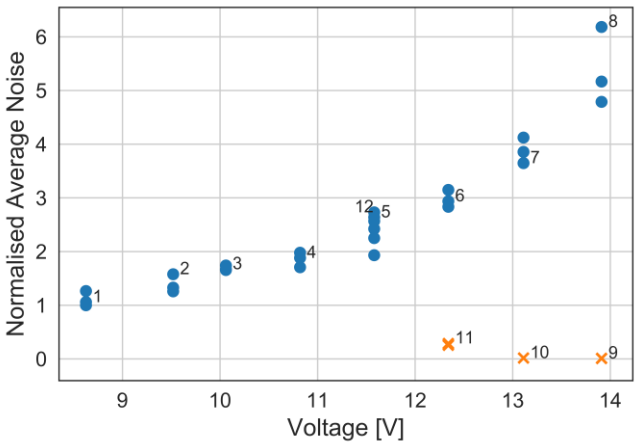

Fig. 12. Voltage – average noise graph for a single microphone with the order of experiments indicated. Orange crosses show captured instances while blue dots show instances without capture

IV. Data Evaluation and Discussion

This section presents the conclusions of the data recorded from both setups and the efficiencies of the achieved separation.

The evaluation of the recorded data from every type of experiment can be classified in 3 different categories:

- Clustering-based algorithm [21]
- ±3 dB points
- Acoustic fingerprint using cosine similarity algorithm

The efficiencies of the various methods in distinguishing records with capture from records without capture are summarised in TABLE I.

TABLE I. Separation efficiency between capture and non-capture states for various evaluation methods

	Separation efficiency		
Clustering based algorithm	***Sensitivity*** 100%	***Response*** 100%	***Noise power*** 100%
Acoustic fingerprint		100%	
± 3dB point based	***Global***		***Individual***
-3 dB point based	93.13%		92.07%
+ 3 dB point based	97.48%		96.09%
±3 dB point based (mismatch excluded)	99.81%		100%

A. Clustering-based algorithm

The data acquired via sensitivity, response magnitude and average noise power measurements were evaluated using algorithms building on clustering method to accurately identify the state of the microphone. An algorithmic approach was required as it was found that a hard threshold is not sufficient in every case to distinguish between response magnitude measured at the lowest V_{bias} and V_{bias} around V_{sb}. The main challenge was discriminating captured records close to the snapback voltage as the records in this region sometimes exhibited a level of sensitivity / response magnitude / noise power, that is close to the ones without capture. The efficiency of the separation for all three datasets was 100%.

B. ±3 dB points

The evaluation of the results based on the ± 3 dB points relies on the magnitude of deviation of the key response parameters from the original pre-capture state. Two different methods were carried out. The first method is a global evaluation method applied on all data used the following hard rules for capture:

- -3 dB points above 100 Hz are considered as capture
- +3 dB points above 17 kHz are considered as capture

To further increase the accuracy of the global evaluation method, the results were separated into capture, no-capture, and uncertain. The uncertain datapoints consist of those that had a mismatch during the evaluation of -3 dB and +3 dB points (for example -3 dB point indicate capture while +3 dB point does not indicate capture). With these mismatched data excluded from the evaluation, the accuracy was increased as shown on the last row of TABLE 1. The second evaluation method looked at the data collected from each microphone individually. The threshold rules were set that only those records were considered capture free that had ± 3 dB points 15% below the average ± 3 dB point values of records with capture.

C. Acoustic fingerprint

The acoustic fingerprint-based evaluation relied on a hard rule regarding the cosine similarity value. As shown in Fig. 10, the records are clearly distinguishable based on their cosine similarity. The following hard rules were applied for capture:

- Records with cosine similarity values above 0.9996 are considered as capture.
- Records with cosine similarity values below 0.9996 are considered as no-capture.

V. Conclusions and Future Work

While lumped element modelling does not possess the accuracy of finite element modelling (FEM), it proved to be sufficient for highlighting the trends in failure mode induced deviations. An advantage of LEM over FEM is its simplicity, not only allowing it to be deployed rapidly, but also making it possible to build it in non-conventional modelling environments, such as python, granting it programmable parameter adjustment capabilities and interaction tools with modern data science techniques. The simulations presented in Section II are in good agreement with the experimental results with regards to all three key performance parameters presented in Section III.

Sweep of the bias voltage of the microphone and measurement of the device response led to the detection of not only the presence of electrostatic capture, but also in the calculation of the voltage ranges for V_{pi} and V_{sb}. This was proven to work both under laboratory conditions and under an in-field configuration with 100% success rate. Moreover, it was demonstrated the determination of critical parameters to avoid capture worked with measuring only the background noise, alleviating the need of an intended audio signal.

In any realistic situation, it cannot be assumed however that the acoustic background noise stays constant during the lifetime of the device, thus condition tracking is not sensible with a

single microphone. However, this problem can be overcome in the case of a multi-microphone setup that is available already in most phones and many smart home devices. If the microphones are located close to each other, the ratio of the noise powers picked up by the devices should stay around the same level. If the ratio changes significantly, the method would pinpoint the faulty device and potentially isolate or repair it [22].

The impact of electrostatic capture was proven to have a clearly distinguishable effect on the ±3 dB points as well that allowed up to 100% separation efficiency on states of capture from no-capture ones. Using solely this information for capture detection needs to be handled with caution as there are various effects, such as lid attach holes or broken diaphragm vents that can influence the low frequency roll-off of a MEMS microphone [23].

The acoustic fingerprint explored in this work proved to be beyond the capabilities of the four-layer framework as such a transducer specific failure signature cannot be reproduced via LEM. Nonetheless, the waveform roughness above 1 kHz is proved to be distinctive for cases of electrostatic capture allowing a detection with 100% accuracy under laboratory conditions. The similarity is present not only regarding the shape of the waveform, but also in terms of its location. It appeared on every recording of captured devices and always at the same frequency range. We suspect that this shape is caused by the membrane touching the dimples of the backplate and is plausibly an effect that is specific to the transducer structure.

Various ways to detect and thus potentially overcome the issue of electrostatic capture of the diaphragm were presented in this article. These solutions are applicable for existing MEMS designs. The fourth layer of the framework was not further explored in detail. Upon the detection of stiction of the diaphragm, an obvious recovery solution is lowering V_{bias} under V_{sb}, then operating the microphone at a value lower than V_{pi}. Other mechanisms to recover from stiction already exist for MEMS [24], however this solution is not suitable for prolonged microphone operation without modification of V_{bias}. As the deviations of the frequency response can be mapped to changes in geometry and/or material properties, detection of modalities beyond the scope of failure modes such as temperature and humidity may be possible along with indicators of long-term degradations such as fatigue. The failure mode simulation, discrimination and recovery layers of the model can therefore be expanded to allow the possibility for detection and potentially compensation for such effects.

ACKNOWLEDGMENTS

We would like to thank Ray Bienek for his help with the setup of the trimming box.

REFERENCES

[1] "JEDEC JESD94A," Application Specific Qualification Using Knowledge Based Test Methodology, 2008.

[2] "JEDEC JEP148A," Reliability qualification of semiconductor devices based on physics-of-failure and risk and opportunity assessment, 2008.

[3] V. Samper and A. Trigg, "MEMS failure analysis and reliability," in Proceedings of the 10th International Symposium on the Physical and Failure Analysis of Integrated Circuits. IPFA 2003, Singapore, 2003, pp. 17–24. doi: 10.1109/IPFA.2003.1222713.

[4] W. Merlijn van Spengen, "MEMS reliability from a failure mechanisms perspective," Microelectronics Reliability, vol. 43, no. 7, pp. 1049–1060, Jul. 2003, doi: 10.1016/S0026-2714(03)00119-7.

[5] W.-C. Chuang, H.-L. Lee, P.-Z. Chang, and Y.-C. Hu, "Review on the Modeling of Electrostatic MEMS," Sensors, vol. 10, no. 6, pp. 6149–6171, Jun. 2010, doi: 10.3390/s100606149.

[6] G. Hantos and M. Desmulliez, "Acoustic methods for detection of specific failure modes in capacitive MEMS microphones," in 2020 IEEE 8th Electronics System-Integration Technology Conference (ESTC), Vestfold, Sep. 2020, pp. 1–8. doi: 10.1109/ESTC48849.2020.9229745.

[7] S. Walser, M. Loibl, M. Winter, C. Siegel, and G. Feiertag, "Sensitivity Recalibration of MEMS Microphones to Compensate Drift and Environmental Influences," Procedia Engineering, vol. 168, pp. 1759–1762, 2016, doi: 10.1016/j.proeng.2016.11.508.

[8] G. Hantos, D. Flynn, and M. P. Y. Desmulliez, "Built-In Self-Test (BIST) Methods for MEMS: A Review," Micromachines, vol. 12, no. 1, p. 40, 2021, doi: 10.3390/mi12010040.

[9] G. Hantos and M. Desmulliez, "Verification and Induction Method for Low Frequency Response Failure Modes in Acoustic MEMS," in 2020 IEEE 33rd International Conference on Microelectronic Test Structures (ICMTS), Edinburgh, May 2020, pp. 1–6. doi: 10.1109/ICMTS48187.2020.9107925.

[10] J. Widder and A. Morcelli, "Basic principles of MEMS microphones," EDN, May 14, 2014. https://www.edn.com/basic-principles-of-mems-microphones/ (accessed May 12, 2020).

[11] J. Lewis, "Understanding Microphone Sensitivity," Analog Dialogue, vol. 46, May 2012, Accessed: Jun. 11, 2020. [Online]. Available: https://www.analog.com/en/analog-dialogue/articles/understanding-microphone-sensitivity.html

[12] M. Pedersen, "A polymer condenser microphone realised on silicon containing preprocessed integrated circuits," University of Twente, 1997.

[13] H. Gharaei and J. Koohsorkhi, "Design and characterization of high sensitive MEMS capacitive microphone with fungous coupled diaphragm structure," Microsyst Technol, vol. 22, no. 2, pp. 401–411, Feb. 2016, doi: 10.1007/s00542-014-2406-2.

[14] S. Shubham and M. Nawaz, "Analysis of Mechanical Sensitivity of MEMS Pressure Diaphragm for Contact Formation," p. 6, 2018.

[15] M. Pedersen, W. Olthuis, and P. Bergveld, "A silicon condenser microphone with polyimide diaphragm and backplate," Sensors and Actuators A: Physical, vol. 63, no. 2, pp. 97–104, Oct. 1997, doi: 10.1016/S0924-4247(97)01532-X.

[16] J. F. McClelland and M. Pedersen, "Capacitive MEMS Microphone Optimized Research," MTEC Photoacoustics Inc AMES IA, Fort Belvoir, VA, Apr. 2005. doi: 10.21236/ADA433689.

[17] L. A. Rocha, E. Cretu, and R. F. Wolffenbuttel, "Hysteresis in the pull-in of microstructures," Proc. MME02, pp. 335--338, 2002.

[18] A. Tellez, M. Pumperla, and M. Malohlava, "Cosine similarity," in Mastering Machine Learning with Spark 2.x, Packt Publishing, 2017.

[19] B.-H. Kim and H.-S. Lee, "Acoustical-Thermal Noise in a Capacitive MEMS Microphone," IEEE Sensors J., vol. 15, no. 12, pp. 6853–6860, Dec. 2015, doi: 10.1109/JSEN.2015.2464372.

[20] S. Walser, C. Siegel, M. Winter, G. Rocca, A. Leidl, and G. Feiertag, "A Novel Method for Reducing the Sensitivity Deviation of MEMS Microphones by Programming," Procedia Engineering, vol. 120, pp. 206–209, 2015, doi: 10.1016/j.proeng.2015.08.611.

[21] J. C. Gower, "A Comparison of Some Methods of Cluster Analysis," Biometrics, vol. 23, no. 4, pp. 623–637, 1967.

[22] Xingguo Xiong, Yu-Liang Wu, and Wen-Ben Jone, "Design and analysis of self-repairable MEMS accelerometer," in 20th IEEE International Symposium on Defect and Fault Tolerance in VLSI Systems (DFT'05), Monterey, CA, USA, 2005, pp. 21–29. doi: 10.1109/DFTVS.2005.30.

[23] G. Hantos and M. P. Desmulliez, "Investigation into Low Frequency Response of Acoustic MEMS for Determination of Failure Modes," IEEE Transactions on Semiconductor Manufacturing, 2021, doi: 10.1109/TSM.2021.3065553.

[24] A. Repchankova and J. Iannacci, "Heat-Based Recovery Mechanism to Counteract Stiction of RF-MEMS Switches," in 2009 Symposium on Design, Test, Integration & Packaging of MEMS/MOEMS, 2009, pp. 176–181.